International Journal of Biological Macromolecules xxx (xxxx) 126279

Contents lists available at ScienceDirect

International Journal of Biological Macromolecules

journal homepage: www.elsevier.com/locate/ijbiomac

Fabrication and characterization of 3D printing biocompatible crocin-loaded chitosan/collagen/hydroxyapatite-based scaffolds for bone tissue engineering applications

Nafiseh Jirofti [a, b, c, 1, 2], Maryam Hashemi [d, e], Ali Moradi [a, b, 2], Fatemeh Kalalinia [b, d, *]

[a] Orthopedic Research Center, Department of Orthopedic Surgery, Ghaem Hospital, Mashhad University of Medical Sciences, Mashhad, Iran
[b] Bone and Joint Research Laboratory, Ghaem Hospital, Mashhad University of Medical Science, Mashhad, Iran
[c] Biotechnology Research Center, Pharmaceutical Technology Institute, Mashhad University of Medical Sciences, Mashhad, Iran
[d] Nanotechnology Research Center, Pharmaceutical Technology Institute, Mashhad University of Medical Sciences, Mashhad, Iran
[e] Departments of Pharmaceutical Biotechnology, School of Pharmacy, Mashhad University of Medical Sciences, Mashhad, Iran

ARTICLE INFO

Keywords:
Crocin
3D printing
Hydroxyapatite
Scaffold
Bone tissue engineering

ABSTRACT

Introduction: Crocin (Cro) is a bioactive biomaterial with properties that promote osteoconduction, osteoinduction, and osteogenic differentiation, making it an ideal candidate for developing mechanically enhanced scaffolds for bone tissue engineering (BTE). Present study focused on a 3D printing matrix loaded with Cro and featuring a composite structure consisting of Chitosan (CH), collagen (Col), and hydroxyapatite (HA).

Method: The scaffolds' structural properties were analyzed using FESEM, and FTIR DSC, while the degradation rate, swelling ratio, cell viability were examined to determine their in vitro performance. Additionally, the scaffolds' mechanical properties were calculated by examining their force, stress, elongation, and Young's modulus.

Results: The CH/Col/nHA scaffolds demonstrated interconnected porous structures. The cell study results indicated that the Cro-loaded in scaffolds cause to reduce the toxicity of Cro. Biocompatibility was confirmed through degradation rate, swelling ratio parameters, and contact angle measurements for all structures. The addition of Cro showed a significant impact on the strength of the fabricated scaffolds. By loading 25 and 50 μl of Cro, the Young's modulus improved by 71 % and 74 %, respectively, compared to the free drug scaffold.

Conclusion: The obtained results indicated that the 3D printing crocin-loaded scaffolds based chitosan/collagen/hydroxyapatite structure can be introduced as a promising candidate for BTE applications.

1. Introduction

Autografts or allografts have been introduced as main bone reconstruction procedures to regenerate defective bone tissue [1]. However, the use of these bone grafts is limited in cases of large or critical-sized bone defects due to various limitations [2]. To address this limitation, researchers have been encouraged to develop bone Tissue Engineering (BTE) as an attractive alternative [3,4]. BTE has demonstrated promising outcomes in enhancing bone regeneration at the defect host site, without causing any morbidity or immunogenicity. BTE relies five crucial factors: 1) generating osteoblasts or other osteogenic cells; 2) mimicking the extracellular matrix (ECM) of the bone using an osteoconductive scaffold; 3) promoting vascularization for nutrient and waste transport, as well as osteoinductive molecule delivery; and 4) utilizing morphogenesis signals to guide cell activation [5].

Several studies have confirmed that Crocin (Cro) plays a crucial role as a bioactive biomaterial in promoting bone regeneration. It possesses osteoconductive, osteoinductive properties, and has been found to facil-

* Corresponding author at: Department of Pharmaceutical Biotechnology, School of Pharmacy, Vakilabad Blvd., Pardis, University Campus, 91886 17871 Mashhad, Iran.
E-mail addresses: JiroftiN4001@mums.ac.ir (N. Jirofti), HashemiM@mums.ac.ir (M. Hashemi), MoradiAL@mums.ac.ir (A. Moradi), kalaliniaf@mums.ac.ir (F. Kalalinia).
[1] First author
[2] Orthopedic Research Center, Department of Orthopedic Surgery, Ghaem Hospital, Mashhad University of Medical Science, P. O. Box 91388-13944, Mashhad, Iran.

https://doi.org/10.1016/j.ijbiomac.2023.126279
Received 7 April 2023; Received in revised form 7 August 2023; Accepted 9 August 2023
0141-8130/

itate the process of osteogenic differentiation of pre-osteocytes and stem cells in BTE [6]. Also, the Cro-loading structure has the potential to create mechanically enhanced scaffolds for bone regeneration applications [7]. It is hypothesized that Cro-loaded scaffolds can be introduced as suitable structures with excellent mechanical and biological properties for BTE.

Chitosan (CH) is a natural biopolymer derived from the deacetylation of polysaccharides found in the shells of marine crustaceans [8]. CH-based bone reconstructions are a potential candidate in regenerative BTE due to their low immunogenicity, biocompatibility, biodegradability, bioresorbable nature and economic feasibility [9]. However, the use of CH scaffolds in BTE is limited by their reduced bioactivity and mechanical properties [10]. To address the aforementioned disadvantage of CH, researchers have explored fabricating CH-based scaffolds in the form of composite structures with other natural or synthetic polymers. They have also investigated incorporating bioactive pharmacological molecules that promote osteogenic differentiation to enhance mechanical properties. These approaches have gained significant attention in this field. [11].

Accordingly, many studies have focused on fabricating composite scaffolds that consist of chitosan, collagen (Col), and nanohydroxyapatite (HA) as these components are considered highly appealing for BTE [12–14]. It is confirmed these scaffolds have the ability to mimic the natural microenvironment of bone tissue [15].

CH, with the hydrophilic surface, is an excellent option in BTE due to its ability to support the attachment and proliferation of bone-forming osteoblast cells [16]. In addition, CH promotes the formation of mineralized bone matrix under in vitro conditions [17]. In this regard, increased knowledge about the organization, structure, and properties of fabricated 3D scaffolds by CH has inspired scientists to design and create innovative biomaterials based on CH and develop novel BTE products.

Col type I is the primary organic constituent of the bone extracellular matrix (ECM) [18,19]. However, Col has some limitations such as simulation of the immune system, high biodegradability, low mechanical strength, and a lack of osteoinductive activity [20]. Therefore, utilizing other biomaterials as morphogenesis signals to guide cell activation and incorporating stronger materials to improve mechanical properties is necessary (Y. [21,22]).

Crocin (Cro) is the main biologically active carotenoid present in saffron, and known for its beneficial properties such as anti-oxidant, anti-apoptotic, and anti-inflammatory effects. Cro has demonstrated the therapeutic potential in arthritis, osteoarthritis, rheumatoid arthritis, and articular pain and treats osteoporosis. Additionally, it has been found to be useful in treating osteoporosis and degenerative diseases [23]. The wide range of activities attributed to crocin is believed to be a result of its ability to bind to multiple proteins, triggering some cellular pathways responsible for mesenchymal stem cell proliferation and differentiation (B. [24]).

Hydroxyapatite (HA), is the primery main component of bone and is a bioceramic with several key advantages including high bioactivity, biocompatibility, biodegradability in physiological conditions, and excellent osteoconductive and osteoinductive capabilities [25–27]. Based on the best of the author's knowledge, fabricated composite scaffolds of CH, Cro, Col, hydroxyapatite (HA) are an osteoconductive matrix can be introduced as improved mechanical and biological structure for BTE.

The 3D-printing method has shown potential applications in the field of bone tissue engineering (BTE) through the use of appropriate bone substitute scaffolds. This technique providing the opportunity to finely control the mechanical and chemical properties and allows for optimal customization to meet specific needs high biodegradabilitys-tructure loaded with Cro that has the potential for bone reconstruction. We focused on optimizing the structure's mechanical, structural, and biological properties while ensuring controlled release of Cro, making it suitable for applications in (BTE).

2. Experimental section

2.1. Materials

Chitosan with low molecular weight (DD = 50,000–190,000) and collagen (type I) was all purchased from Sigma-Aldrich, Germany. Sodium chloride (NaCl), Potassium dihydrogen phosphate (KH_2PO_4), Potassium chloride (KCl), Sodium phosphate monobasic dihydrate ($NaH_2PO_4{\cdot}2H_2O$), and Glacial Acetic acid (99.7 %) were purchased from Merck (Germany). For in vitro study fetal bovine serum (FBS), alamar blue, and Dulbecco's modified Eagle's medium (DMEM) were purchased from Gibco (USA). Cor powder was obtained from Sami Labs Limited, Bengaluru, India. All chemicals were used as received without further purification.

2.2. Preparation of the polymeric bioink

A CH/nHA bioink was prepared by dissolving 1.7 g of CH (17%w/v) and 0.68 g of nHA powder in acetic acid (80 %) for 24 h at room temperature using the magnetic stirrer (600 rpm). Subsequently, 0.625 g of Col (7 % wt.) was prepared in acetic acid (80 %) for 2 h at 4 °C. At the final stage, the Col solution was slowly added to the Cho/nHA bioink, and mixed for 2 h at 4 °C.

2.3. Fabrication and stabilization of 3D printing CH/ Col/nHA scaffolds

The scaffolds were fabricated by 3D printing process from 56 % of CH solution (17%w/v) containing 24 % of nHA and 20 % of Col (7 % wt.) solution. Square scaffolds ($20 * 20 * 5$ mm^3) were printed with 0°–90° orientation of the filaments and 3 % fill density in alternate layers. The schematic in Fig. 1 shows the printing set-up and depicts the printing process. The structures were fabricated using a custom-modified 3D printer (Pishgaman Sazeh Nano-zist Comp- IRAN, Tabriz) with two controlled extruders. The G-code with a 0°–90° pattern was utilized for nozzle movement to print and obtain rectangular pores. To establish chemical bonds between CH and Col, the scaffolds were immersed in a 5%wt. NaOH solution for 30 min. In this condition, most of the single-bond NH_3^+ groups on CH chains were deprotonated into single-bond NH_2 groups upon contact with NaOH, through the action of single-bond OH ions [28]. To eliminate residual NaOH, the cross-linked scaffolds were rinsed three times with deionized water. Finally, the fabricated scaffolds were frozen in a dryer for up to 24 h under −80 °C temperature and 5 bar pressure conditions.

2.4. Cro loading in scaffolds

The scaffolds were subjected to a water uptake capacity test, and based on the obtained results; all scaffolds were soaked in 25 and 50 μM of Cro solution and incubated in a shaker incubator at 40 rpm and 37 °C for approximately 6 h. Next, the scaffolds were freeze-dried and stored in a dark place at room temperature.

2.5. Characterization of 3D printing scaffolds

2.5.1. Scanning Electron Microscope Imaging (FE-SEM) and porosity measurement

At the first, all scaffolds were coated by gold and platinum thne structure of the fabricated scaffolds was examined using scanning electron microscopy imaging (FE-SEM). The samples were cut using a punch and fixed to an adhesive carbon stub before being imaged with a TableTop SEM (Hitachi High-Technologies Corp., Japan) operated at 15 kV. To obtain vertical section imaging, the samples were fractionated along the vertical direction by immersing them in liquid nitrogen.

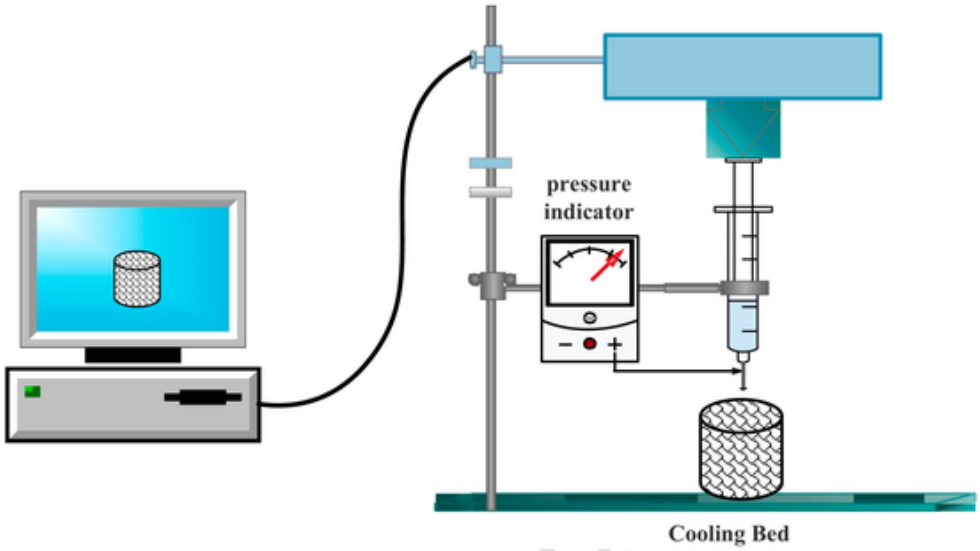

Fig. 1. A schematic diagram of 3D printing set up.

The porosity of the 3D printing scaffolds was measured using the gravimetric method. Eqs. (1) and (2) were used to determine apparent density and porosity, respectively:

$$\text{Apparent density of the scaffold} = \frac{\text{mat mass } (gr)}{\text{mat thickness } (cm) \times \text{mat area } (cm^2)} \quad (1)$$

$$\text{Porosity } (\%) = 1 - \frac{\text{apparent density of the scaffold } \left(\frac{gr}{cm^3}\right)}{\text{bulk density of solution } \left(\frac{gr}{cm^3}\right)} \times 100 \quad (2)$$

2.6. Infrared Fourier Transfer Analysis (FTIR)

To confirm the functional groups and identify the types of bonds present between CH, Col, nHA, and Cro in the fabricated scaffolds, Fourier transform infrared (FTIR) analysis was conducted. All of the experiments were performed by Thermo Nicolet spectrometer AVATAR 370 FTIR (Waltham, MA) within the wavelength range of 400–4000 cm^{-1}.

2.7. Mechanical properties

The H50KS universal testing machine (Hounsfield, UK) was applied to examine of the mechanical properties of 3D printing scaffolds. For this purpose, fabricated structures were cut into strips (10 mm × 10 mm × 4 mm) and immersed in PBS (pH 7.4) for 30 min. The scaffolds were placed into the grips of the machine and subjected to a 100 N load cell while the crosshead speed was set at 5 mm/min, until they reached their breaking point.

2.8. In vitro studies

2.8.1. Drug encapsulation efficiency

For encapsulation efficiency measurement certain amount of the Cho/nHA/Col/Cro 25 and Cho/nHA/Col/Cro 50 scaffolds dissolved in acetic acid at room temperature and was stirred and sonicated for 1 day to release Cro into acetic acid. The amount of free Cro was evaluated by UV spectrophotometer at 298 nm. Calibration a curve of drug was performed by diluting the difference concentrations of Cro in phosphate buffered saline (pH 7.4). Finally the drug encapsulation efficiency (EE%) and drug loading capacity (DL%) were evaluated by following equations:

$$\text{Drug encapsulation efficiency } (EE\%) = \frac{\text{amount of Crosin loading in scaffold}}{\text{total amount of used Crosin for encapsulation}} \times 100$$

2.9. Drug release assay

The Cro release profile from Cho/Nha/Col/Cro 25 and 50 scaffolds was determined by floating the certain amount of fabricated scaffolds in 2 ml of PBS (pH 7.5). The immersed samples incubated in a shaker incubator at 37 °C and in difference time step (1, 2, 3, 4, 24, 48, and 72 h) 100 μl of the solution was transferred from each sample to the test tube and replaced with 100 μl of fresh PBS solution. The concentration of released Cro was assessed by a UV spectrophotometer (Shimadzu UV-1700 PharmaSpec, Kyoto, Japan) at 440 nm. Finally, the concentration of Cro at each time point was evaluated by the standard calibration curve and expressed as the percent of cumulative drug released.

2.10. Degradation Test

The degradation rate of 3D printing scaffolds ($n = 5$) was determined by immersing the scaffolds in phosphate buffer saline (PBS) with pH 7.4 and placed in a shaker incubator at 37 °C. The weight loss percentage of the samples was measured at regular intervals of 1, 3, 5, 7, 12, 21, and 24 days using Eq. (3):

$$\text{Degredation rate}\% = \left[\left(W_1 - W_2\right)/W_1\right] \times 100 \quad (3)$$

W_1 = First Weight
W_2 = Second Weight at specific time of study

2.11. Swelling ratio

To evaluate the swelling ratio of fabricated 3D printing scaffolds (CH/Col/nHA, Cho/Col/nHA/Cro 25, CH/Col/nHA/Cro 50) preweighed dry scaffolds (W) were immersed in a PBS buffer at 37 °C and incubated for 6, 12, 18, and 24 h. After the incubation, the swollen scaffolds were weighed (W_1) and the water uptake capacity was calculated by the following equation (Eq. (4)):

$$WC\ (\%) = \frac{W_1 - W}{W} \times 100 \quad (4)$$

2.12. Contact angle

Water contact angle measurement was used to evaluate the hydrophilicity of both free and drug-loaded 3D printing scaffold. Accordingly, distilled water (5 μl) was dropped on the surface of scaffolds (n = 5) and the contact angle was recorded after using images were taken with a digital camera at 3 s at room temperature.

2.13. Cell study

2.13.1. Toxicity study

The cytotoxicity of fabricated scaffolds ($n = 4$) on L929 cells was evaluated by Alamar Blue assay. The punched scaffolds were placed in the plate (96 well), and sterilized with UV. The L929 (density of 5×10^3 cells/well) were seeded on the scaffolds containing DMEM, 10 % FBS and 1 % penicillin-streptomycin and incubated in a humidified incubator at 37 ˚C with 5 % CO_2. The free cells with the complete medium were set as a control sample. At 1, 3, 5, and 7 days the alamar blue (10 μl) was added to each well and incubated for 4 h for 3 h at 37 ˚C and 5 % CO_2. The alamar blue absorption was detected at 605 nm by an ELISA reader (BioTek, Bad Friedrichshall, Germany). Finally, the percentage of cell growth was calculated through the following formula:

$$\%The\ growth\ rate\ compared\ to\ control\ sampl = \frac{Test\ sample\ absorbance}{Control\ sample\ absorbance\ (cell\ alone)} \times 100 \quad (5)$$

2.13.2. Cell proliferation and morphology examination against 3Dprinting scaffolds

Cell attachment and proliferation against fabricated scaffolds (free drug and drug-loaded) was examined by L929 cells. For this purpose, cells (density of 5×10^3 cells/well) were seeded on the scaffolds in a 48-well plate containing completed medium (DMEM, 10 % (*v*/v) FBS, and 1 % (v/v) penicillin-streptomycin), and incubated in a humidified incubator at 37 ˚C with 5 % CO_2 for 1, 3, 5, and 7 days. All samples were fixed by adding 4 % (w/v) formaldehyde solution to each well (for 30 min). In the following, dehydration of scaffolds was done with different concentrations of alcohol (100, 90, 80, 70, and 60), respectively, for 15 min.

The cell morphology on fixed scaffolds were evaluated using an inverted light microscope (Olympus IX50; Olympus, Tokyo, Japan), at 10× magnification by the obtained images (surface and cross) were taken by a digital camera.

2.14. Statistical calculations

All of the results were stated in mean ± SD (standard deviation). The data were analyzed by SPSS software (21.0). ANOVA followed by Tuckey's Post Hoc test were used to compare the outcomes of different groups. In this study, a *P*-value <0.05 was considered as significant.

3. Results

3.1. Morphological examination using FE-SEM images

The Field Emission Scanning Electron Microscopes (FE-SEM) images of the 3D printing scaffolds are shown in Fig. 2. All scaffolds resulted in a uniformed structure. The large pore size and good porosity observed

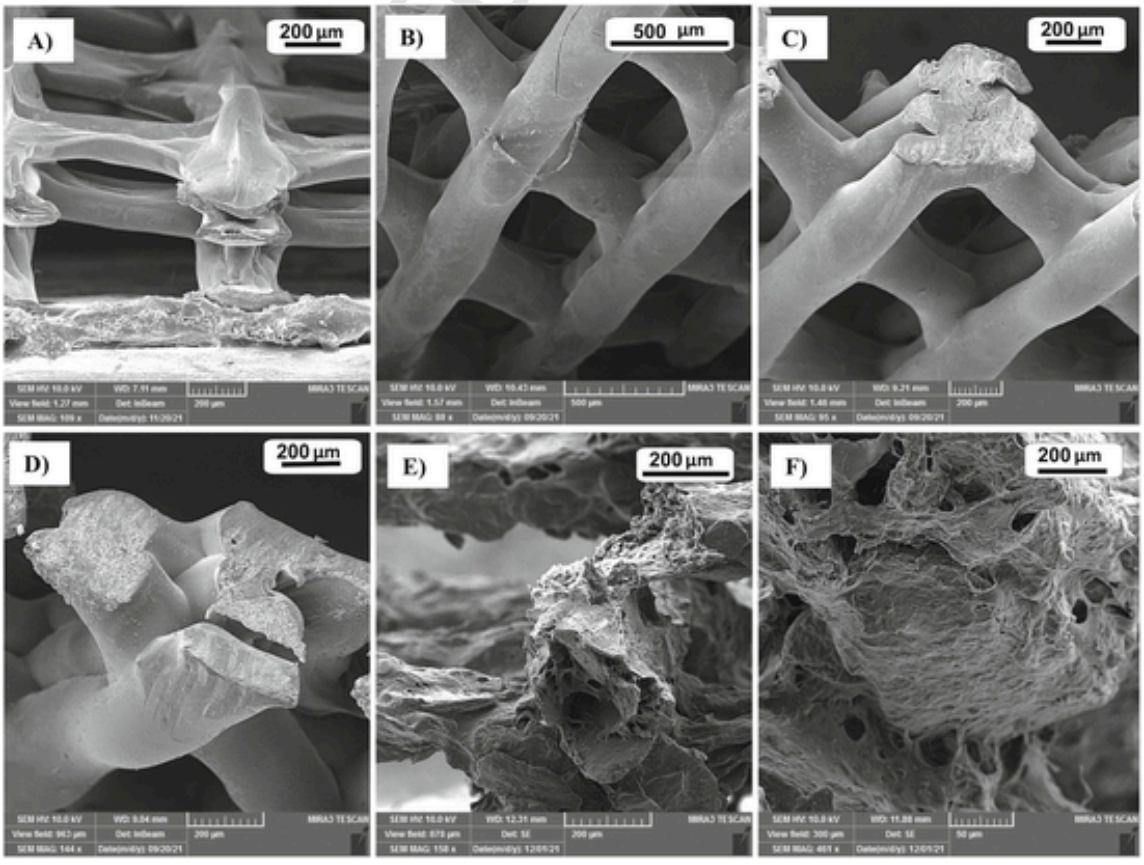

Fig. 2. Field Emission Scanning Electron Microscopes (FE-SEM) images of the 3D printing CH/Col/nHA scaffolds are taken at, A) 200×,B), 500×, C) 200×, D) 200×,E) 200×, and F) 50×.

can be attributed to the lyophilization process, evidenced by the pores on the printed filaments. Additionally, all structures displayed a homogeneous surface characteristic.

3.2. Porosity measurement

The 3D printing process was employed to fabricate the CH/Col/nHA scaffolds, which demonstrated well-controlled and interconnected porous structures. The mean porosity was measured for the CH/Col/nHA, CH/Col/ nHA/Cro 25, and Cho/Col/nHA/Cro 50 scaffolds at 58.0 ± 2.8 %, 89.4 ± 0.87 %, and 90.0 ± 0.97 %, respectively (Table 1). The significant difference was observed between free drug to drug-loaded scaffolds.

3.3. Fourier transform infrared (FTIR) spectroscopy

The FTIR spectra of CH, Col, nHA, CH/Col/nHA, CH/Col/nHA/Cro 25 and CH/Col/nHA/Cro 50 were obtained in the range of 400–4000 cm^{-1} (with KBr). Details regarding the characteristic board of different functional groups of transmission bands and the relative intensities (ΔT %) are presented in Fig. 3 and Table 2.

The asymmetric stretching vibration of phosphate (P—O) present in HA appeared at 1030 cm^{-1}, while the band at 605 and 565 cm^{-1} confirms the presence of symmetric stretching vibration of phosphate (P—O). The peak observed at 3358 cm^{-1} was due to the hydrogen bond stretching in OH ions present in CH. The symmetric stretching vibration of CH_2 present in CH appeared at 2883 cm^{-1}. The peaks appeared at 1656, 1540 cm^{-1} were attributed to amide I(C=O), amide II (–NH) groups in Col, which is very similar to CH respectively. The C—O, –C=O, O—H bands with vibrational modes, were detected at 1103–1112 cm^{-1}, 1622–1637 cm^{-1}, and 3418–3445 cm^{-1}, respectively.

Table 1
Porosity of CH, Col, CH/Col, nHA, CH/Col/nHA, and CH/Col/nHA /Cro 25 and 50 structures.

Sample	Porosity (%)
CH/COL/HA	58.0 ± 2.8
CH/COL/HA/Cro 25	89.4 ± 0.87
CH/COL/HA/Cro 50	90.0 ± 0.97

3.4. Evaluation of mechanical properties of 3D printing scaffolds

Fig. 4 and Table 3 displays the mechanical properties, including force, stress, elongation, and Young's modulus, of CH/Col/nHA, CH/Col/nHA/Cro 25, and CH/Col/nHA/Cro 50. The stress and module young of fabricated scaffolds in 25 % and 50 % of Cro-laoded scaffold show 19 % and 29 % (stress), and 79 % and 74 % (young module) increases compared to CH/Col/nHA as a control sample. These results suggest that adding Cro to the CH/Col/nHA scaffold can increase force, stress, and Young's modulus. The extension of the drug-loaded scaffold was reported 51.95 ± 14.5 % which is lower than the free drug scaffold (125.031 ± 56.4 %). However, there was no significant difference between obtained results of force, stress, and extension. Meanwhile, the strength of free drug and drug-loaded was determined, and adding Cro caused a significant difference in strength compared to CH/Col/nHA as a control sample.

3.5. In vitro analysis

3.5.1. Drug encapsulation efficiency

Based on the experimental data, the EE% was determined to be 76.7 ± 1.5 % for CH/COL/HA/Cro 25 and 79.2 ± 3.5 % for CH/COL/HA/Cro 50 scaffolds.

3.5.2. Drug release assay

The Cro release profile of CH/COL/HA/Cro 25 and CH/COL/HA/Cro 50 is shown in Fig. 5. The release profile showed that the burst release of the drug was occurred after 5 h of incubation for both structures. Mean-while, Cro released from CH/COL/HA/Cro 25 showed slower release kinetics compared to CH/COL/HA/Cro 50. For CH/COL/HA/ Cro 25 scaffold there exists an initial burst phase within the five hour of incubation, in which up to ca. 46 % of the drug was released and then, it progressively leveled off to reach ca. 38 % of total drug after 48 h of incubation. For CH/COL/HA/ Cro 50 a similar profile is observed, but up to ca. 56 % of the bioactive cargo was released during the burst phase within the first hour and reaching ca. 44 % after 144 h, respectively.

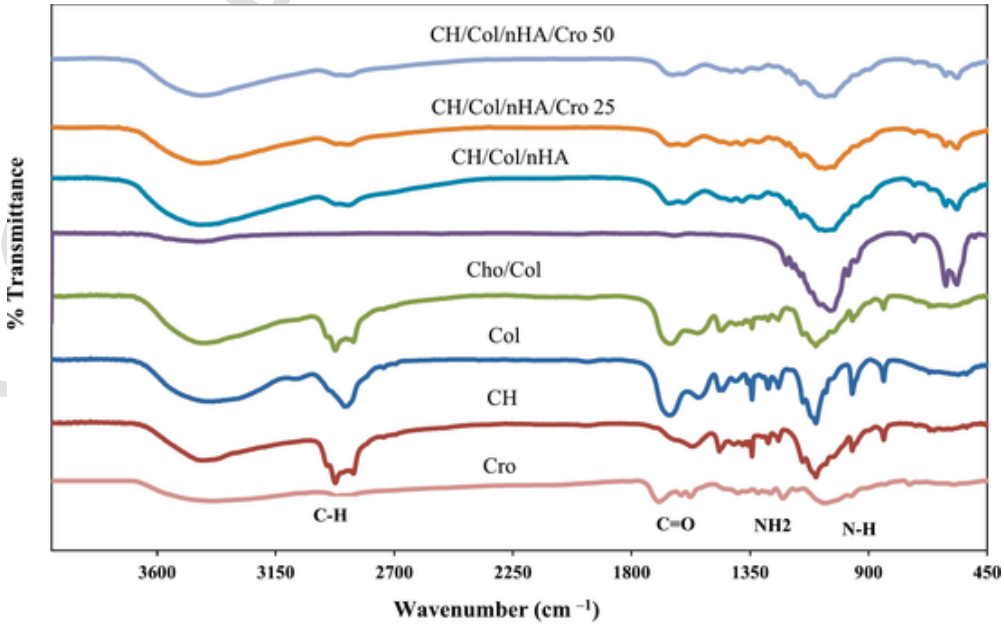

Fig. 3. The FT-IR spectrum of CH, Col, CH/Col, nHA, CH/Col/nHA, and CH/Col/nHA /Cro 25 and 50 structures.

Table 2
Characteristic board of different functional groups of transmission bands and the relative intensities (ΔT %) of CH, Col, CH/Col, nHA, CH/Col/nHA, and CH/Col/nHA /Cro 25 and 50 structures.

Vibration group	Type of vibration	Wave number (cm^{-1})	ΔT (%)						
			CH	Col	Cro	HA	CH/Col/HA	CH/Col/ha/Cro25	CH/Col/ha/Cro25
–OH; N–H	Stretching	3418–3445	59	55	54	–	42	47	52
$–CH_2$; –C–H	Stretching in an acid	2918–2923	36	59	60	–	70	81	82
$–CH_3$, CH_2	Stretching	2852–2880	45	–	61	–	72	83	83
–C=O	Stretching	1722–1724	95	75	62	–	89	94	96
–C=O	Stretching	1622–1637	81	53	63	–	73	81	84
$–CH_2$	Bending	1452–1466	74	63	65	–	73	81	84
–C–H; –C–C	Bending in plane	1409–1411	77	76	65	–	76	83	88
–C–N	Stretching	1384	77	81	64	–	73	81	84
–C–OH	Stretching	1244–1275	81	70	62	83	80	86	91
–C–O–C	Vibrating	1103–1112	32	41	56	23	45	58	63
$–CH_2$; –C–H	Rocking; bend out plane	713–729	17	5	74	96	93	95	96

3.5.3. Degradation

The degradation rate of CH/Col/nHA, CH/Col/nHA/Cro 25, CH/Col/nHA/Cro 50 scaffolds are presented in Fig. 6. The results indicate that the drug-loaded scaffolds exhibited a lower rate of degradation compared to the Cho/nHA/Col scaffold, which was used as the control sample.

Over the course of the study (1 to 24 days), the degradation rate increased for all three types of scaffolds. Specifically, for the Cho/nHA/Col scaffold, the degradation rate increased from 13 % to 26.03 %, while for the Cho/nHA/Col/Cro 25 and Cho/nHA/Col/Cro 50 scaffolds, the degradation rate increased from 3.5 % to 15.18 % and from 3.67 % to 13.47 %, respectively.

Notably, the highest and lowest degradation rates were observed in the CH/Col/nHA scaffold (26.03 ± 1.46 %) and the CH/Col/nHA/Cro 50 scaffold (13.47 ± 0.46 MPa), respectively, with a significant difference between free drug and drug-loaded scaffolds ($p < 0.05$).

3.5.4. Swelling ratio

The swelling ratio of the fabricated 3D printing scaffolds at 6, 12, 18, and 24 h are shown in Table 4**.** All structures showed higher capacity compare to free drug structure as a control sample. In other words, by increasing the Cro in the structure the swelling ratio decreased from 168.73 ± 8.95 to 178.35 ± 3.31 (for Cho/nHA/Col/Cro 25) and to 198.5 ± 2.31 (for Cho/nHA/Col/Cro 50) after 6 h. A significant difference was observed between the swelling ratio after 6 h and 18 h ($p < 0.05$).

3.5.5. Contact angle

The results of the contact angle of the 3D printed scaffolds (CH/Col/nHA, CH/Col/nHA/Cro 25, CH/Col/nHA/Cro 50) was presented in the Fig. 7. The contact angle of free drug and drug-loaded scaffolds was reported 35 ± 0.3, 30 ± 1.5, and 27 ± 1.4 respectively, without any significant difference between all scaffolds. Fig. 7 confirms that loading Cro into the scaffolds resulted in a decrease in the contact angle.

3.6. Cell study

3.6.1. Toxicity assay

The cell viability of all components in composite structures of 3D printing and fabricated scaffolds (with and without Cro) were reported in Fig. 8. The cell toxicity was not observed in fabricated scaffolds. Free

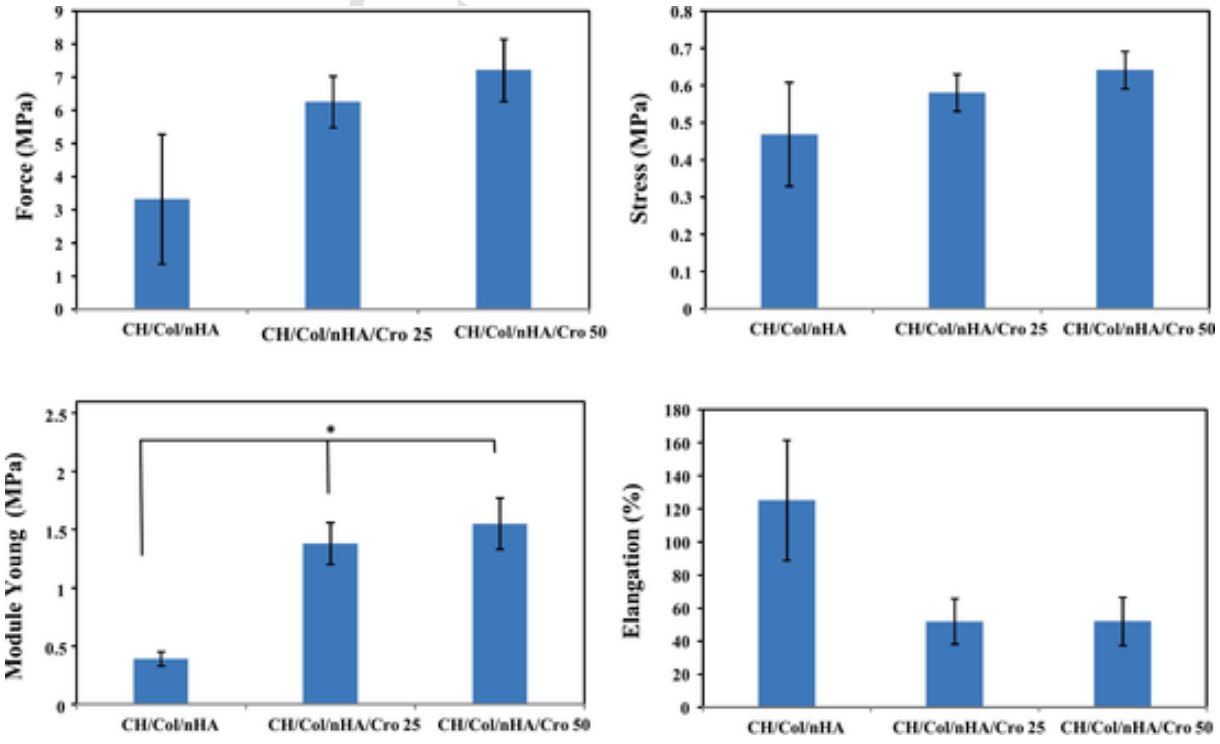

Fig. 4. Mechanical properties (Force, Stress, Young Module, and Elongation) of CH/Col/nHA, CH/Col/nHA/Cro 25, and CH/Col/nHA/Cro 50 scaffolds, *P*-value is defined as*,#, $ means $P < 0.05$ comparison with control sample. P-value is defined as* $P < 0.05$ compared with control sample (CH/Col/nHA).

Table 3
Mechanical properties (Force, Stress, Module Young, and Elongation) of CH/Col/nHA, CH/Col/nHA/Cro 25, and CH/Col/nHA/Cro 50 scaffolds.

Sample	Force (N)	Extension (mm)	Stress (Mpa)	Elongation (%)	Elongation at break (%)	Young's modulus (Mpa)
CH/COL/HA	3.313 ± 1.96	2.89 ± 0.88	0.468 ± 0.24	125.031 ± 56	46.619 ± 24.63	0.39 ± 0.06
CH/COL/HA/Cro 25	6.25 ± 0.77	2.29 ± 0.51	0.58 ± 0.05	51.78 ± 13	11.86 ± 9.4	1.38 ± 0.48
CH/COL/HA/Cro 50	7.21 ± 0.94	2.09 ± 0.22	0.641 ± 0.05	51.95 ± 14	29.56 ± 28.66	1.55 ± 0.23

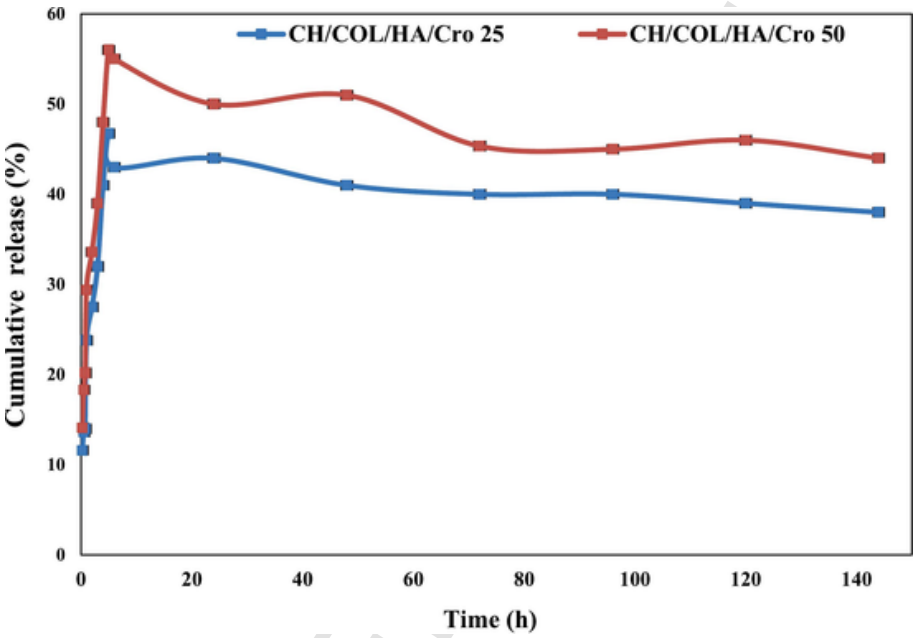

Fig. 5. Release profiles of of CH/COL/HA/Cro 25 and CH/COL/HA/Cro 50 in PBS (pH: 7.4) at 37 °C for 144 h.

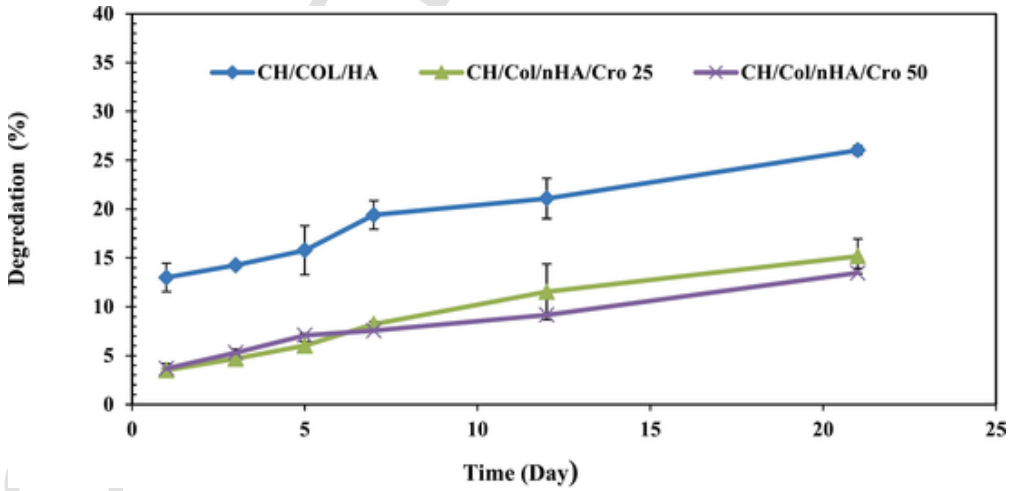

Fig. 6. Degradation rate of CH/Col/nHA, CH/Col/nHA/Cro 25, and CH/Col/nHA/Cro 50 scaffolds in phosphate buffer saline (PBS) with pH 7.4 in a shaker incubator at 37 °C at 1, 3, 5, 7, 12, 21, and 24 days.

Table 4
Swelling ratio of CH/Col/nHA, CH/Col/nHA/Cro 25, and CH/Col/nHA/Cro 50 scaffolds in phosphate buffer saline (PBS) with pH 7.4 at 6, 12, and 18 h.

Sample	6 h	12 h	18 h
Cho/nHA/Col	283.53 ± 22.01	257.01 ± 15.21	168.73 ± 18.95
Cho/nHA/Col/ Cro 25	298.23 ± 11.03	274.35 ± 9.21	174.35 ± 13.31
Cho/nHA/Col/Cro 50	328.01 ± 9.30	311.24 ± 9.01	198.5 ± 21.31

drug (Cro) showed lower cell viability (40.59 ± 9.9 %) and CH/Col/nHA/Cro 25 (110.2 ± 11.25 %) scaffold indicated higher cell viability compare to all scaffold, after 7 days. The different concentrations (5, 20, and 50 wt%) of pure nHA, in the time study, indicated higher cell viability compared to the free cells with the complete medium as a control sample. Control sample, especially at 3 and 7 days of toxicity assay. In cell viability examinations of the drug-loaded scaffolds, there is not any significant difference at 1, 3, 5, and 7 day between different concentrations of Cro. All drug-loaded scaffolds showed higher cell viability (96.5 ± 15.2 % for CH/Col/nHA/Cro 25 and 77.2 ± 3.1 % for CH/Col/nHA/Cro 25) compared to free-drug scaffold (79.3 ± 3.4 % for

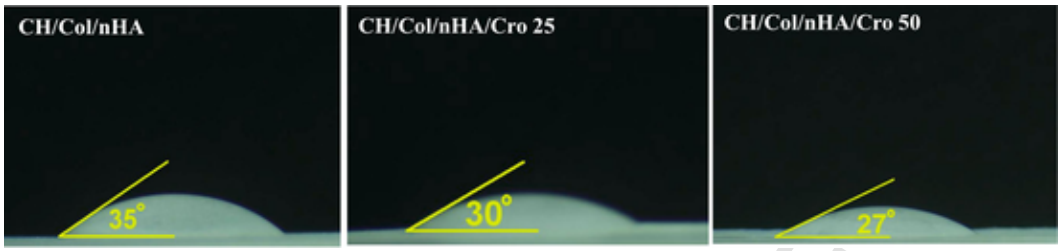

Fig. 7. Contact angle measurement of CH/Col/nHA, CH/Col/nHA/Cro 25, CH/Col/nHA/Cro 50 scaffolds by dropping water on the surface of the all 3D-printing scaffolds.

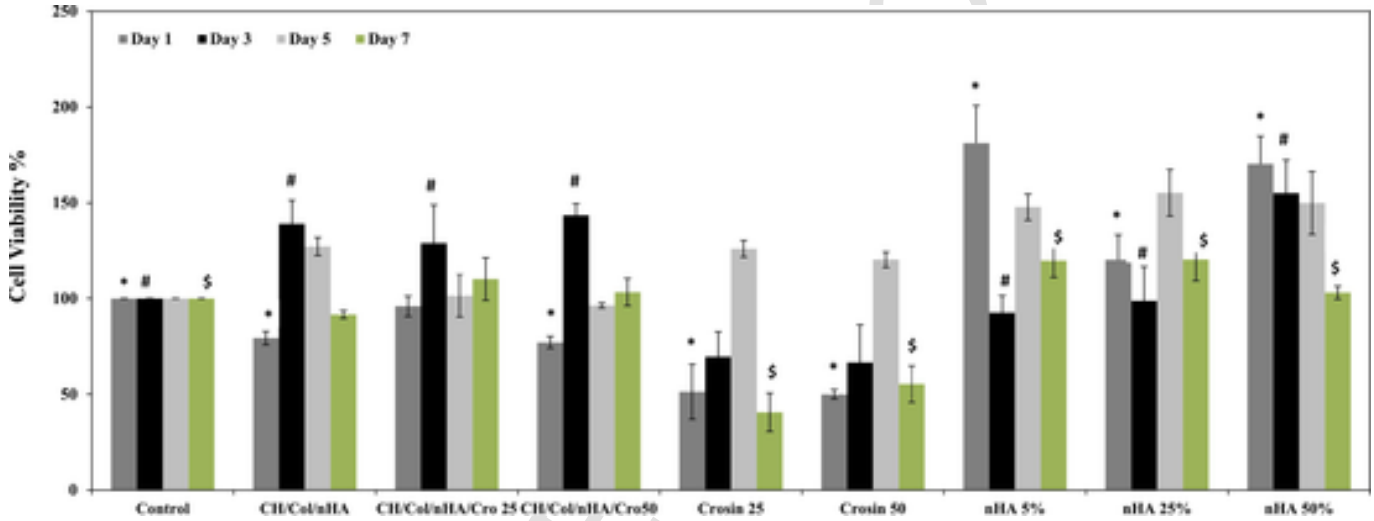

Fig. 8. Evaluation of cell viability of fibroblast (L929) cell cultured on CH/Col/nHA, CH/Col/nHA/Cro 25, CH/Col/nHA/Cro 50, Cro 25 and Cro 50, nHA5%, nHA25%, and nHA50%. Cells cultured in medium only were assumed as control samples. *P*-value is defined as *, #, $ $P < 0.05$ in compared with control sample. All results are expressed as means ± SD (Tuckey's Post Hoc test, $n = 4$). P-value is defined as*,#, $ means $P < 0.05$ compared to the free cells with the complete medium as a control sample..

CH/Col/nHA) as the control sample. The Fig. 8 shows a clear representation of all significant differences.

3.6.2. Cell morphology examination

Cell attachment and proliferation of 3Dprinting scaffolds (CH/Col/nHA, CH/Col/nHA/Cro 25, and CH/ Col/nHA/Cro 50) were presented in Fig. 9.

Based on the obtained images all scaffolds indicated the good cell attachment and normal cell morphology. According to the morphological features of cells, any undergo late-stage apoptosis and cell death in cell morphology was not observed.

4. Discussion

Chitosan and collagen are two widely used natural polymers with unique properties that make them ideal for bone repair and BTE [29]. It is reported that Cro can enhance cell proliferation and differentiation of mesenchymal stem cells by anchoring to proteins [30]. Moreover, Cro with anti-inflammatory properties shows effective therapeutic potential in treating osteoporosis and degenerative bone diseases [31]. It is confirmed, that using the 3D printing technique to fabricate degradable, biocompatible, porous scaffolds with the ability to assemble by cell and growth factors can achieve BTE [32]. In this regard, the main objective of the present study was to fabricate 3D printing scaffolds with osteoconductivity properties suitable for BTE. To achieve this, CH/Col/HA scaffolds were initially fabricated using 3D printing techniques. Subsequently, different concentrations (25 and 50 macro-molar) of Cro were loaded into the fabricated scaffolds.

The obtained FESEM images confirmed the homogeneity of the inks, distribution of the printed material, and suitable phase separation. The smooth surface structure of the fabricated composite is attributed to the use of Col, which is in agreement with previous findings reported by Nagaraj et al. [33]. The FTIR spectra of both the free drug and drug-loaded structures confirmed the presence of functional groups from all components in the 3D fabricated scaffold, without any undesirable reactions. In addition, characteristic bands were shifted to higher wavenumber in Cro-loaded scaffold. Also In tissue engineering, it is crucial to consider various parameters such as swelling ratio, degradation rate, and the ability to load drugs and specific growth factors when designing ideal scaffolds. Additionally, porosity plays a vital role in creating scaffolds with optimal water capacity, degradation profile, and high drug encapsulation capacity [34]. The 3D printing process leads to fabricating of porous scaffolds with interconnected porosity [35]. The CH/Col/nHA scaffold exhibited satisfactory porosity and the addition of Cro was found to increase the porosity in drug-loaded scaffolds due to high topological polar surface area and molecular volume of Cro [36,37]. According to the obtained results, fabricated scaffold with more porosity showed higher drug loading. It is hypothesized that the speed, quality, and quantity of tissue regeneration will be improved by controlling drug delivery in structure [38]. In this article, drug-loaded scaffolds showed slow and controllable release rates. This is a crucial objective for enhancing drug efficacy while minimizing the risks of potential side effects [39]. In simpler terms, using 3D-printed scaffolds as drug delivery system allows for optimal conditions for drug delivery. Mechanical strength is a critical parameter that defines a scaffold's performance in BTE. Moreover, studies have reported that Cro can enhance the longitudinal and perpendicular forces of bone [7]. Our study has shown that

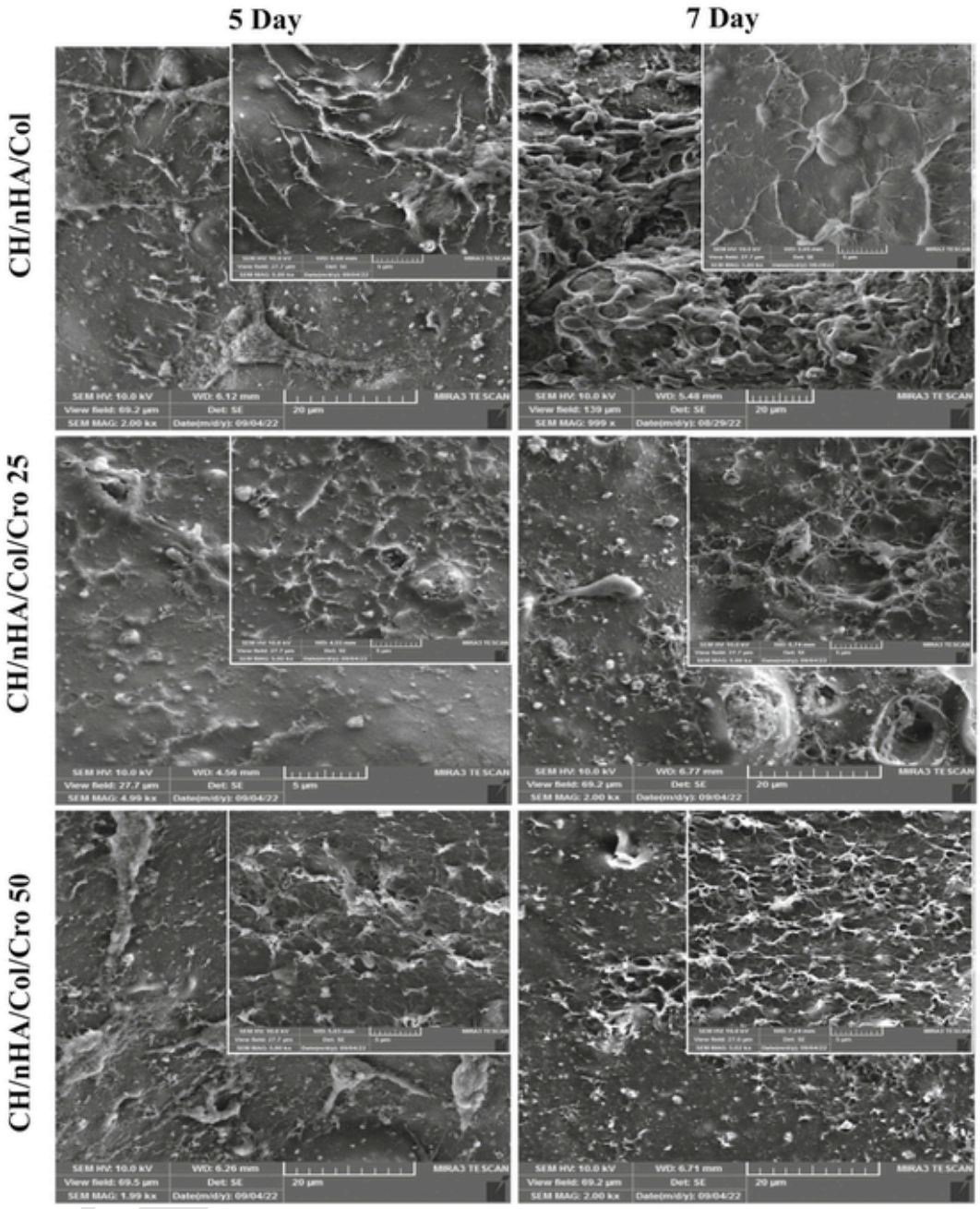

Fig. 9. Optical microscopy images CH/Col/nHA, CH/Col/nHACro 25, and CH/ Col/nHA/Cro 50 in L929 cells after 5 and 7 Day. (Magnification: 20×).

incorporating Cro into 3D-printed scaffolds leads to an increase in force, stress, and Young's modulus. Furthermore, the presence of HA in the scaffolds contributes to their overall strength. The reconstruction of damaged bones using artificial scaffolds that bear the closest resemblance to bones has garnered significant attention in BTE, as per reported results. Bone regeneration is achieved through the degradation and absorption of these artificial scaffolds. The swelling ratio is influenced by factors such as the degree of crosslinking, components used, porosity, and architecture of the printed meshes. The evaluation of degradation rate is crucial for determining the replacement rate of scaffolds with new tissue, without any residual material remaining [40]. The degradation rate of drug-loaded scaffolds decreased compared to free-drug scaffolds. Also, it is observed which Cro-loading scaffold showed higher strength compared to CH/Col/nHA scaffold. The degradation behavior of CH/Col/nHA/Cro can be attributed to the enzymatic breakdown of CH and Col, but the incorporation of Cro, which enhances mechanical properties, has been shown to reduce the rate of degradation in structures fabricated using 3D printing. The cytotoxicity examination indicated lower toxicity of drug-loaded scaffolds compared to free drugs. In other words, more cell viability in Cro-loaded scaffolds confirmed the reduction of the toxicity of natural drugs by their encapsulation which is in agreement with the reported results by Rahnama et al. [41]. The cell morphology analysis did not show any undesirable changes suggestive of apoptosis or cell death in the L929 cells. This indicates that the three-dimensional (3D) printed CH/Col/HA/Cro 50 scaffolds have great potential as a viable alternative for BTE when autografts or allografts are not feasible.

5. Conclusion

In this study, a 3D printing process was used to prepare chitosan/collagen/nano-hydroxyapatite scaffolds loaded with Cro. All scaffolds

confirmed suitable structure properties without undesirable functional group in drug loading scaffolds. Loading of Cro into CH/Col/nHA structure increased the swelling ratio and strength while decreasing the degradation rate of the scaffold. Moreover, the drug-Loaded structure showed improved biocompatibility by decreasing the contact angle. Furthermore, the drug-loaded scaffolds displayed the lower toxicity compared to the free Cro and all scaffolds displayed normal cell morphology of and all scaffolds displayed a normal cell morphology on L929 cell lines. Considering to the obtained results, the CH/Col/HA/Cro 50 structure can introduce as a practical topical drug delivery system for BTE applications.

Abbreviations

BTE	Bone tissue engineering
Cro	Crocin
CH	Chitosan
Col	Collagen
3D	three-dimensional
DMEM	Dulbecco's modified Eagle's medium
ECM	Extracellular matrix
FBS	Fetal bovine serum
HA	Hydroxyapatite ()
FTIR	Infrared Fourier Transfer Analysis
KH_2PO_4	Potassium dihydrogen phosphate
KCl	Potassium chloride
NaCl	Sodium chloride ()
$NaH_2PO_4{\cdot}2H_2O$	Sodium phosphate monobasic dihydrate
FE-SEM	Scanning Electron Microscope Imaging

Ethics approval

Not applicable.

Consent for publication

Not applicable.

Funding

This work was supported financially by the Vice-Chancellor for Research of Mashhad University of Medical Sciences, Mashhad, Iran.

Consent to participate

Not applicable.

Code availability

Not applicable.

CRediT authorship contribution statement

Nafiseh Jirofti: Study design, Investigation, Data collection, Conceptualization, Writing - Original Draft, prepared all Figures and Tables.

MaryamHashemi: Investigation, Resources.

Ali Moradi: Investigation, Resources.

Fatemeh Kalalinia: Review & Editing, Supervision, Resources, Funding acquisition, Project administration

Declaration of competing interest

The author(s) declared no potential conflicts of interest with respect to the research or publication of this article.

Data availability

The data sets used and/or analyzed during the current study are available from the corresponding author on request.

Acknowledgments

The authors are grateful to the Research Council of Mashhad University of Medical Sciences, Mashhad, Iran, for approval and financial support of this project.

References

[1] Rosa S. Valtanen, Yunzhi P. Yang, Geoffrey C. Gurtner, William J. Maloney, David W. Lowenberg, Synthetic and bone tissue engineering graft substitutes: what is the future? Injury 52 (2021) S72–S77, https://doi.org/10.1016/j.injury.2020.07.040.

[2] Emil H. Schemitsch, Size matters: defining critical in bone defect size!, J. Orthop. Trauma 31 (2017) S20–S22, https://doi.org/10.1097/BOT.0000000000000978.

[3] Ami R. Amini, Cato T. Laurencin, Syam P. Nukavarapu, Bone tissue engineering: recent advances and challenges, Crit. Rev. Biomed. Eng. 40 (5) (2012), https://doi.org/10.1615/CritRevBiomedEng.v40.i5.10.

[4] Cameron R.M. Black, Vitali Goriainov, David Gibbs, Janos Kanczler, Rahul S. Tare, Richard O.C. Oreffo, Bone tissue engineering, Curr. Mol. Bio. Rep. 1 (2015) 132–140, https://doi.org/10.1007/s40610-015-0022-2.

[5] Guoke Tang, Zhihong Tan, Wusi Zeng, Xing Wang, Changgui Shi, Yi Liu, Xiaojian Ye, Recent advances of chitosan-based injectable hydrogels for bone and dental tissue regeneration, Front. Bioeng. Biotechnol. 1084 (2020), https://doi.org/10.3389/fbioe.2020.587658.

[6] Caitlin McKenzie Koski, Biological and Mechanical Performance of 3D Printed Composite Scaffolds and Assessment of Chemopreventative and Anti-Inflammatory Agents for Bone Tissue Engineering, Washington State University, Applications, 2019.

[7] Mardi M. Algandaby, Crocin attenuates metabolic syndrome-induced osteoporosis in rats, J. Food Biochem. 43 (7) (2019) e12895, https://doi.org/10.1111/jfbc.12895.

[8] Fatemeh Kalalinia, Zhila Taherzadeh, Nafiseh Jirofti, Nafise Amiri, Neda Foroghinia, Mona Beheshti, Elham Pishavar, Evaluation of wound healing efficiency of vancomycin-loaded electrospun chitosan/poly ethylene oxide nanofibers in full thickness wound model of rat, Int. J. Biol. Macromol. 177 (2021) 100–110, https://doi.org/10.1016/j.ijbiomac.2021.01.209.

[9] Antonia Ressler, Chitosan-based biomaterials for bone tissue engineering applications: a short review, Polymers 14 (16) (2022) 3430, https://doi.org/10.3390/polym14163430.

[10] Wuren Bao, Menglu Li, Yanyu Yang, Yi Wan, Xing Wang, Na Bi, Chunlin Li, Advancements and frontiers in the high performance of natural hydrogels for cartilage tissue engineering, Front. Chem. 8 (2020) 53, https://doi.org/10.3389/fchem.2020.00053.

[11] Sheeny K. Lan Levengood, Miqin Zhang, Chitosan-based scaffolds for bone tissue engineering, J. Mater. Chem. B 2 (21) (2014) 3161–3184, https://doi.org/10.1039/C4TB00027G.

[12] José Becerra, Mariano Rodriguez, Dayana Leal, Karem Noris-Suarez, Gema Gonzalez, Chitosan-collagen-hydroxyapatite membranes for tissue engineering, J. Mater. Sci. Mater. Med. 33 (2) (2022) 18, https://doi.org/10.1007/s10856-022-06643-w.

[13] Erivelto Luís Chacon, Mirella Romanelli Vicente Bertolo, de Guzzi Plepis, Ana Maria, da Conceição Amaro Martins, Virginia, Dos Santos, Geovane Ribeiro, Clovis Antônio Lopes Pinto, Fabricio Montenegro Nazari, Collagen-chitosan-hydroxyapatite composite scaffolds for bone repair in ovariectomized rats, Sci. Rep. 13 (1) (2023) 28, https://doi.org/10.1038/s41598-022-24424-x.

[14] Ayşe Karakeçili, Serdar Korpayev, Kaan Orhan, Optimizing chitosan/collagen type I/nanohydroxyapatite cross-linked porous scaffolds for bone tissue engineering, Appl. Biochem. Biotechnol. 194 (9) (2022) 3843–3859, https://doi.org/10.1007/s12010-022-03962-0.

[15] Mirella Romanelli Bertolo, Martins Vicente, Virginia Conceição Amaro, de Guzzi Plepis, Ana Maria., Effects of calcium phosphates incorporation on structural, thermal and drug-delivery properties of collagen: chitosan scaffolds, Int. J. Adv. Med. Biotechnol. 2 (2) (2019) 25–35, https://doi.org/10.25061/2595-3931/IJAMB/2019.v2i2.32.

[16] Nafiseh Jirofti, Mohadese Golandi, Jebrail Movaffagh, Farajollah Shahriari Ahmadi, Fatemeh Kalalinia, Improvement of the wound-healing process by curcumin-loaded chitosan/collagen blend electrospun nanofibers: in vitro and in vivo studies, ACS Biomater. Sci. Eng. 7 (8) (2021) 3886–3897, https://doi.org/10.1021/acsbiomaterials.1c00131.

[17] Yang-Jo Seol, Jue-Yeon Lee, Yoon-Jeong Park, Yong-Moo Lee, Young Ku, In-Chul Rhyu, Chong-Pyoung Chung, Chitosan sponges as tissue engineering scaffolds for bone formation, Biotechnol. Lett. 26 (13) (2004) 1037–1041, https://doi.org/10.1023/B:BILE.0000032962.79531.fd.

[18] Nafiseh Jirofti, Davod Mohebbi-Kalhori, Ramin Masoumi, Enhancing biocompatibility of PCL/PU nano-structures to control the water wettability by NaOH hydrolysis treatment for tissue engineering applications, J. Ind. Text. 1528083720963268 (2020), https://doi.org/10.1177/1528083720963268.

[19] Jebreil Movaffagh, Bibi Sedigheh Bazzaz, Taherzadeh Fazly, Hashemi Zhila, Moghaddam Maryam, Atieh Seyedian, Seyyed abbas Tabatabaee, Nafiseh Jirofti, Evaluation of wound-healing efficiency of a functional Chitosan/Aloe vera hydrogel on the improvement of re-epithelialization in full thickness wound model of rat, J. Tissue Viab. 31 (4) (2022) 649–656, https://doi.org/10.1016/j.jtv.2022.07.009.
[20] Gholamhosein Kazemzadeh, Nafiseh Jirofti, Kazemi Mehrjerdi, Rajabioun Hosein, Alamdaran Masoud, Seyed Ali, Davod Mohebbi-Kalhori, Reza Taheri, A review on developments of in-vitro and in-vivo evaluation of hybrid PCL-based natural polymers nanofibers scaffolds for vascular tissue engineering, J. Ind. Text. 52 (2022) 15280837221128314, https://doi.org/10.1177/15280837221128314.
[21] Youbin Li, Yuzhe Liu, Ronghang Li, Haotian Bai, Zhengqing Zhu, Liwei Zhu, Jincheng Wang, Collagen-based biomaterials for bone tissue engineering, Mater. Des. 210 (2021) 110049, https://doi.org/10.1016/j.matdes.2021.110049.
[22] Gustavo A. Rico-Llanos, Sara Borrego-González, Miguelangel Moncayo-Donoso, José Becerra, Rick Visser, Collagen type I biomaterials as scaffolds for bone tissue engineering, Polymers 13 (4) (2021) 599, https://doi.org/10.3390/polym13040599.
[23] Shayan Vafaei, Xuming Wu, Jiajie Tu, Seyed Noureddin Nematollahi-Mahani, The effects of crocin on bone and cartilage diseases, Front. Pharmacol. 12 (2021) 830331, https://doi.org/10.3389/fphar.2021.830331.
[24] Borui Li, Kairong Qin, Benjie Wang, Baoyi Liu, Weiting Yu, Zhigang Li, Dewei Zhao, Crocin promotes osteogenesis differentiation of bone marrow mesenchymal stem cells, Dev. Biol. 56 (8) (2020) 680–688, https://doi.org/10.1007/s11626-020-00487-w.
[25] Sudip Mondal, Umapada Pal, Apurba Dey, Natural origin hydroxyapatite scaffold as potential bone tissue engineering substitute, Ceram. Int. 42 (16) (2016) 18338–18346, https://doi.org/10.1016/j.ceramint.2016.08.165.
[26] Mehrnoush Nakhaei, Nafiseh Jirofti, Mohammad H. Ebrahimzadeh, Ali Moradi, Different methods of hydroxyapatite-based coatings on external fixator pin with high adhesion approach, Plasma Process. Polym. e 2200219 (2023), https://doi.org/10.1002/ppap.202200219.
[27] Hongjian Zhou, Jaebeom Lee, Nanoscale hydroxyapatite particles for bone tissue engineering, Acta Biomater. 7 (7) (2011) 2769–2781, https://doi.org/10.1016/j.actbio.2011.03.019.
[28] Wei Chang, Fei Liu, Hafiz Rizwan Sharif, Zhengnong Huang, H. Douglas Goff, Fang Zhong, Preparation of chitosan films by neutralization for improving their preservation effects on chilled meat, Food Hydrocoll. 90 (2019) 50–61.
[29] Kai Wang, Yanen Wang, Xinpei Li, Chi Zhang, 3D printing of hydroxyapatite/chitosan and collagen scaffolds for bone tissue engineering, Front. Bioeng. Biotechnol. (2016), https://doi.org/10.3389/conf.FBIOE.2016.01.01286.
[30] Reyhane Hoshyar, Homa Mollaei, A comprehensive review on anticancer mechanisms of the main carotenoid of saffron, crocin, J. Pharm. Pharmacol. 69 (11) (2017) 1419–1427, https://doi.org/10.1111/jphp.12776.
[31] M. Hemshekhar, M. Sebastin Santhosh, K. Sunitha, R.M. Thushara, K. Kemparaju, K.S. Rangappa, K.S. Girish, A dietary colorant crocin mitigates arthritis and associated secondary complications by modulating cartilage deteriorating enzymes, inflammatory mediators and antioxidant status, Biochimie 94 (12) (2012) 2723–2733, https://doi.org/10.1016/j.biochi.2012.08.013.
[32] Qiliang Zhang, Jian Zhou, Peixuan Zhi, Leixin Liu, Chaozong Liu, Ao Fang, Qidong Zhang, 3D printing method for bone tissue engineering scaffold, Med. Novel Technol. Dev. 100205 (2023), https://doi.org/10.1016/j.medntd.2022.100205.
[33] Anushree Nagaraj, Alaitz Etxabide Etxeberria, Rafea Naffa, Ghada Zidan, Ali Seyfoddin, 3D-printed hybrid collagen/GelMA hydrogels for tissue engineering applications, J. Biol. 11 (11) (2022) 1561, https://doi.org/10.3390/biology11111561.
[34] Gholamhosein Kazemzadeh, Nafiseh Jirofti, Davod Mohebbi-Kalhori, Farkhonde Sarhaddi, Reza Taheri, Pathological examination of blended and co-electrospinning hybrid polycaprolactone/polyurethane nanofibers for soft tissue engineering applications, J. Ind. Text. 51 (4_suppl) (2022) 6816S–6837S, https://doi.org/10.1177/15280837221074070.
[35] Sophie C. Cox, John A. Thornby, Gregory J. Gibbons, Mark A. Williams, Kajal K. Mallick, 3D printing of porous hydroxyapatite scaffolds intended for use in bone tissue engineering applications, Mater. Sci. Eng. C 47 (2015) 237–247, https://doi.org/10.1016/j.msec.2014.11.024.
[36] Susmita Bose, Sahar Vahabzadeh, Amit Bandyopadhyay, Bone tissue engineering using 3D printing, Mater. Today 16 (12) (2013) 496–504, https://doi.org/10.1016/j.mattod.2013.11.017.
[37] Kamal Essifi, Mohamed Brahmi, Doha Berraaouan, Abderrahim Ed-Daoui, El Bachiri, Fauconnier Ali, Marie-Laure, Abdesselam Tahani, Influence of sodium alginate concentration on microcapsules properties foreseeing the protection and controlled release of bioactive substances, J. Chem. 2021 (2021) 1–13.
[38] Kunal J. Rambhia, Peter X. Ma, Controlled drug release for tissue engineering, J. Control. Release 219 (2015) 119–128, https://doi.org/10.1016/j.jconrel.2015.08.049.
[39] Aneeza Rani, Muhammad Asgher, Sarmad Ahmad Qamar, Nimrah Khalid, Nanostructure-mediated delivery of therapeutic drugs—a comprehensive review, Int. J. Chem. Biochem. Sci. 15 (2019) 5–14, https://doi.org/10.3390/molecules26195905.
[40] Pamela Habibovic, Uwe Gbureck, Charles J. Doillon, David C. Bassett, Clemens A. van Blitterswijk, Jake E. Barralet, Osteoconduction and osteoinduction of low-temperature 3D printed bioceramic implants, Biomaterials 29 (7) (2008) 944–953, https://doi.org/10.1016/j.biomaterials.2007.10.023.
[41] Shahrbanoo Rahnama, Jebrail Movaffagh, Azadeh Shahroodi, Nafiseh Jirofti, Fazly Bazzaz, Bibi Sedigheh, Monir Beyraghdari, Fatemeh Kalalinia, Development and characterization of the electrospun melittin-loaded chitosan nanofibers for treatment of acne vulgaris in animal model, J. Ind. Text. 52 (2022) 15280837221112410, https://doi.org/10.1177/15280837221112410.